




Cite this: *Chem. Commun.*, 2021, 57, 13126

Received 29th September 2021,  
Accepted 12th November 2021

DOI: 10.1039/d1cc05483j

rsc.li/chemcomm

# A facile design of thio-perylenediimides with controllable fluorescent, photodynamic and photothermal effects towards cancer theranostics†

Chang Liu, Chendong Ji, Zongyang Fan, Ruihao Ma and Meizhen Yin \*

**A series of thionated perylenediimides with modulating phototheranostic modalities have been synthesized by a one-pot method for multiple anti-cancer applications. Compared to the initial and 4-*tert*-butyl phenol-substituted fluorescent perylenediimide, the obtained mono-thionated perylenediimide became photodynamic. With the increase of thionation degree, tetrathionated perylenediimide changed into an optimal photothermal agent.**

Phototheranostics, including fluorescence/photoacoustics imaging and photodynamic/photothermal therapy (PDT/PTT),<sup>1–4</sup> have shown great potential in fighting tumors. For example, perylenediimides (PDIs) with excellent photostability and variable photophysical properties have been applied in multifunctional phototheranostics of tumors.<sup>5–7</sup> Typically, heavy atoms, metal atoms or amino groups should be introduced and conjugated to PDIs to enhance their photodynamic or photothermal ability through the enhancing of nonradiative decays.<sup>8–10</sup> However, their on-demand applications are still limited because of their nonadjustable and uncontrollable phototheranostics and complex syntheses.<sup>11–13</sup> Therefore, in order to have PDIs with controllable phototheranostics, it is essential to have a precise method to systematically manipulate their fluorescent, photoacoustic, photodynamic and photothermal properties.

Currently, heavy-atom-free modification of PDIs has received much attention in the construction of photosensitizers (PSs) as antitumor medicines.<sup>14,15</sup> For example, the substitution of carbonyl groups with sulfur atoms could increase the electron affinity, rapid triplet formation or thermal deactivation pathway of the PDI chromophore.<sup>16–22</sup> However, the relationship between the degree of thionation and photophysical

properties of substituted PDIs has not been reported and needs further investigation.

Herein, 4-*tert*-butyl phenol-substituted PDI (PDI-O) was chosen as the initial compound because of its four carbonyl sites to easily regulate the degree of thionation. We successfully synthesized a series of sulfur atom substituted PDIs with a one-pot method as potential phototheranostics having different thionation degrees. The relationship between the phototheranostic ability and the thionation degree showed that the monothionated PDI (PDI-1S) became photodynamic from the original fluorescent PDI-O. With the increase of thionation degree, their <sup>1</sup>O<sub>2</sub> quantum yields were gradually reduced while their photothermal conversion efficiencies were gradually increased. The tetrathionated PDI (PDI-4S) also became an optimal photothermal agent. Therefore, excitation energy dissipation pathways of PDIs in the phototheranostics of tumors could be manipulated through only one-step sulfur substitution (Scheme 1).

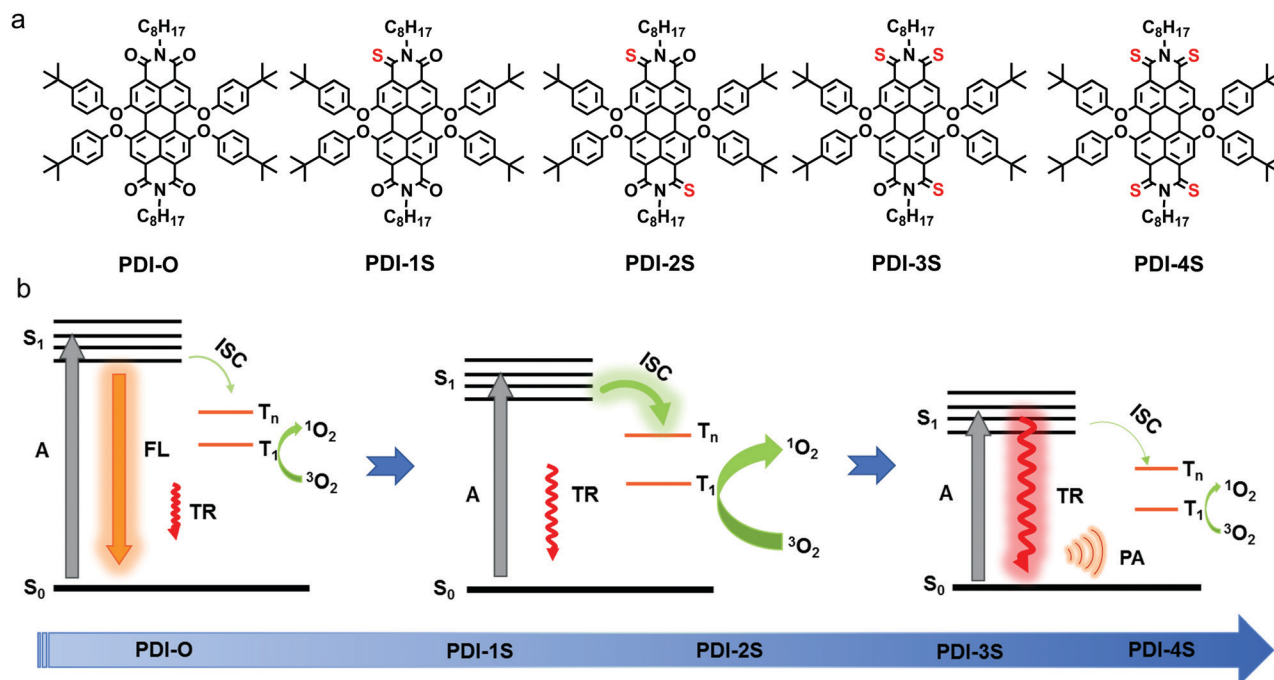
According to the reported method,<sup>23</sup> the thionated PDI derivatives (PDI-1S–4S) were synthesized from a one-pot microwave reaction between the parent PDI-O and commercial Lawesson's reagent within 20 min (Fig. S1, ESI†). These compounds were further systematically characterized by <sup>1</sup>H and <sup>13</sup>C NMR spectroscopy and mass spectroscopy (Fig. S2–S14, ESI†).

As listed in Table 1, the increase of sulfur atoms in PDI-O–4S caused gradient red shifts of the absorption peak from 575 nm to 769 nm, which was in agreement with that from theoretical calculations (Fig. 1a and Table 1). The maximum absorption redshift was 194 nm approximately due to the effective decrease of the energy gap between the HOMO and LUMO (Table 1 and Fig. S15, ESI†).<sup>24</sup> The redshift in absorption could deepen the tissue penetration<sup>25</sup> and increase the maximum permissible exposure (MPE) to skin, which led to an improved phototheranostic effect.<sup>26</sup> Furthermore, although PDI-O had an excellent fluorescence emission (Fig. 1b), PDI-1S–4S were almost non-fluorescent ( $\Phi_{\text{PL}} \approx 0.00$ ) (Table 1).

According to the fluorescence quenching, other energy relaxation pathways, intersystem crossing or thermal deactivation, might exist.<sup>27–29</sup> Subsequently, 1,3-diphenylisobenzofuran

State Key Laboratory of Chemical Resource Engineering,  
Beijing Laboratory of Biomedical Materials,  
Beijing University of Chemical Technology, Beijing 100029, China.  
E-mail: yinmz@mail.buct.edu.cn

† Electronic Supplementary Information (ESI) available: Experimental procedure, <sup>1</sup>H and <sup>13</sup>C NMR spectrum, mass spectroscopy, absorption spectra, fluorescence spectra, photodynamic and photothermal supplementary data, etc. See DOI: 10.1039/d1cc05483j



**Scheme 1** (a) Chemical structures of thionated PDIs, and (b) schematic illustration of manipulating phototheranostic effects through the controlling of thionation degree (A: absorption, FL: fluorescence, TR: thermal radiation, ISC: intersystem crossing, PA: photoacoustic).

**Table 1** Photophysical and photosensitizing properties of thionated PDI compounds

PDIs	$\lambda_{\text{abs}}^a/\text{nm}$	$\Phi_{\text{PL}}^{bf}$	$\Phi_A^c/\%$	$E_g^d/\text{eV}$	$R(\times 10^6)^e$
O	575	0.92	1.0	2.31	0.13
1S	623	<i>f</i>	95.6	2.13	8571.67
2S	666	<i>f</i>	45.8	1.99	2639.46
3S	719	<i>f</i>	11.1	1.81	2271.76
4S	769	<i>f</i>	0.5	1.68	126.32

<sup>a</sup> Measured in dichloromethane (DCM). <sup>b</sup> Fluorescence quantum yield in DCM. <sup>c</sup> Singlet oxygen quantum yield ( $\Phi_A$ ) determined according to MB ( $\Phi_A = 57\%$  in DCM). <sup>d</sup> Calculated from  $E_g = 1240/\lambda_{\text{abs}}$  ( $E_g$  is the energy difference between the HOMO and LUMO level). <sup>e</sup>  $R = [(S|H_{\text{SO}}|T)/\Delta E_{\text{ST}}]^2$ . <sup>f</sup> Not observed.

(DPBF) was employed as a probe to measure the  $^1\text{O}_2$  generation. Compared with the photosensitizer methylene blue (MB) as the standard, the evaluated singlet oxygen quantum yields ( $\Phi_A$ ) of PDI-O–S4 showed that  $\Phi_A$  was gradually decreased with the increase of thionation degree (Table 1), in which PDI-1S had the maximum singlet oxygen signal with  $\Phi_A \approx 0.96$  (Fig. 1c), while PDI-4S had the lowest with  $\Phi_A \approx 0.005$  under the same conditions (Fig. S16, ESI†). In order to further understand the mechanism, theoretical calculations were carried out on the optimized structures of PDI-O–4S to study the formation energy from the single state to triplet state. The formation of  $^1\text{O}_2$  was found to be directly proportional to the ISC rate constant ( $k_{\text{ISC}}$ ),<sup>30</sup> and  $k_{\text{ISC}}$  was related to the singlet–triplet energy gap ( $\Delta E_{\text{ST}}$ ) (Table S1, ESI†) and the spin–orbit coupling (SOC) constants (Table S2, ESI†), which could be described with the relevant equation.<sup>31</sup> The value representing the overall ISC

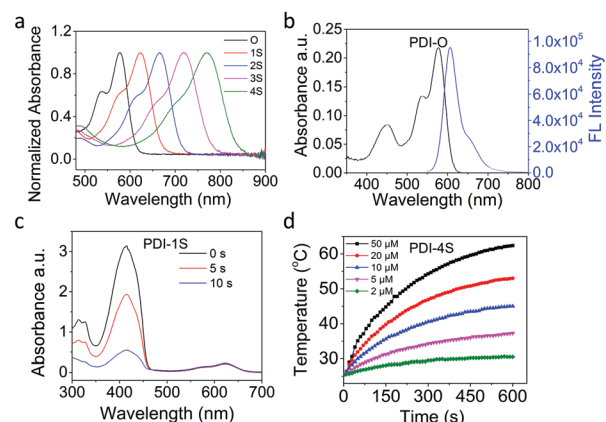


**Fig. 1** (a) Vis-NIR absorption spectra of thionated PDIs, (b) fluorescent spectra of PDI-O (in dichloromethane (DCM),  $\lambda_{\text{ex}}$  at the 535 nm), (c) photochemical oxidation of 1,3-diphenylisobenzofuran (DPBF) with  $^1\text{O}_2$  generated from PDI-1S in DCM (650 nm red light irradiation, 5 mW cm<sup>−2</sup>), and (d) photothermal heating curves of PDI-4S NP solutions at different concentrations (2, 5, 10, 20 and 50 μM) under 808 nm laser irradiation at a power of 1 W cm<sup>−2</sup>.

process of PDI-1S was the largest, which was consistent with the measured singlet oxygen quantum yield (Table S3, ESI†). Mono-thionated PDIs had the prominent  $^1\text{O}_2$  quantum yield due to their rapid triplet formation. However, it was found that the rate of intersystem crossing was negatively related to the degree of thionation, and the photophysical properties of compounds with higher thionation degree should be further investigated. Because the organic optical agents with red-shifted absorption usually

avored nonradiative thermal deactivation pathways,<sup>32,33</sup> redder-absorbing agents with more sulfur atom replacement should have improved photothermal properties.

In order to confirm the photothermal generation, water-soluble nanoparticles (PDI-O-4S NPs) were prepared under the same conditions with the commercial amphiphilic triblock copolymer F127 as the coating agent in the nano-coprecipitation method. The formed spherical PDI-O-4S NPs had average diameters of  $138.21 \pm 1.86$  nm,  $134.01 \pm 1.27$  nm,  $127.66 \pm 1.66$  nm,  $157.46 \pm 0.73$  nm and  $126.62 \pm 0.27$  nm, respectively (Fig. S17 and S18, ESI†). As the result of the same F127 coating, the zeta potentials of PDI-O-4S NPs are similar, which are  $-13.66 \pm 0.51$  mV,  $-13.22 \pm 2.39$  mV,  $-12.15 \pm 1.73$  mV,  $-10.96 \pm 0.99$  mV and  $-12.13 \pm 1.04$  mV, respectively (Fig. S19, ESI†). Additionally, these nanoparticles could be stable with unchanged diameters in phosphate buffer solutions (PBS) and cell culture medium (DMEM) for two weeks at 4 °C, which was needed for long-term circulation *in vivo* (Fig. S20, ESI†). The as-prepared PDI-O-4S NPs displayed a red shift of 22–34 nm in the absorption spectrum compared with that of PDI-O-4S in organic solvent, which benefited a deeper penetration (Table S4 and Fig. S21, ESI†).

Although PDI-O NPs had an excellent fluorescence emission (Fig. S22, ESI†), PDI-1S-4S NPs had no fluorescence emission in aqueous solution. According to their  $^1\text{O}_2$  generation and photothermal performance of PDI-1S-4S NPs in water, PDI-1S NPs maintained the best singlet oxygen quantum yield (58.5%) (Fig. S23 and Table S4, ESI†), and the calculated photothermal conversion efficiency ( $\eta$ ) of PDI-1S-4S NPs were 27.2%, 30.1%, 32.3% and 46%, respectively (Fig. S24, ESI†). The  $\eta$  was calculated by a steady-state heating and natural cooling curve. Based on the quantification method developed by Roper,<sup>36</sup> detailed calculation of the  $\eta$  value was presented in the ESI†. With the increase of thionation degree, there was a gradual upward trend of  $\eta$  (Table S4, ESI†). Because the photoacoustic (PA) signal usually had a positive correlation with the photothermal ability,<sup>37,38</sup> they could be plotted in a normalized phantom mold. In this study, PDI-4S NPs had the best PA signal intensity in aqueous solution (Fig. S25, ESI†) due to their largest redshift in the absorption spectrum and the best photothermal performance. Their specific photothermal heating effect of PDI-4S NPs had a positive correlation to their concentration and laser power (Fig. 1d and Fig. S26, ESI†). As shown in Fig. 2a and b, the PA signal intensity of PDI-4S NPs was increased with the increase of their concentration. Furthermore, the results showed that PDI-4S NPs had excellent and stable photothermal and PA performance in aqueous solution without photobleaching after multiple laser irradiation (Fig. S27, ESI†), which should lead them to an excellent theranostic effect under complex physiological conditions.

The tested *in vitro* properties of PDI-O showed that it had the best fluorescence performance and could be used as a fluorescence imaging probe. PDI-1S had the best photodynamic ability due to its energy dissipation dominated by rapid ISC process, and could be used in tumor phototherapy. PDI-4S, having the most redshifted absorption, favored nonradiative thermal deactivation, and could be used as a photothermal and PA agent in tumor theranostics.

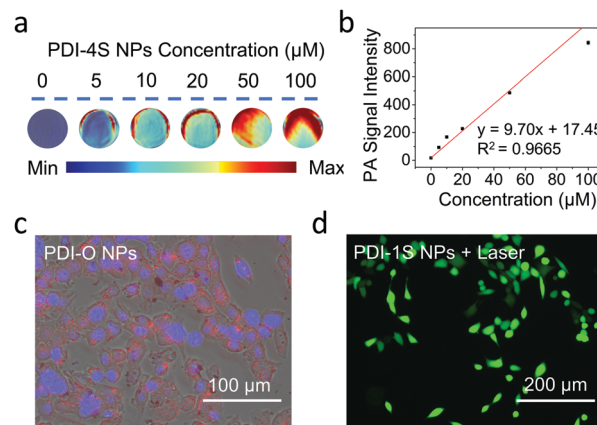


Fig. 2 (a and b) Photoacoustic (PA) images and corresponding PA signal intensity of PDI-4S NPs as a function of concentration, (c) fluorescence images of 4T1 cells stained with PDI-O NPs (5  $\mu\text{M}$ ), and (d)  $^1\text{O}_2$  generation of 4T1 cells co-cultured with PDI-1S NPs (10  $\mu\text{M}$ ) with dichlorofluorescein diacetate (DCF-DA) as a  $^1\text{O}_2$  probe (error bars, mean  $\pm$  SD).

After the thionated PDIs were applied in tumor cells with a Cell Counting Kit-8 (CCK-8) assay to examine their dark cytotoxicity, their negligible cytotoxicity was found even at concentrations of 100  $\mu\text{M}$  (Fig. S28, ESI†), indicating that the thionated PDI NPs had excellent biocompatibility with a great potential in phototheranostic applications. After the co-culture of the murine breast cancer (4T1) cells with PDI-O NPs for 12 h, red fluorescence was observed under the fluorescence microscope, which proved that PDI-O NPs had excellent fluorescence imaging capability *in vitro* (Fig. 2c and Fig. S29a, ESI†). Furthermore, after 4T1 cells were stained with  $^1\text{O}_2$  probe and irradiated with a NIR laser after the co-incubation with PDI-1S-4S NPs, DCF (green) fluorescence appeared compared with other groups, suggesting that  $^1\text{O}_2$  was produced from PDI-1S NPs *in vitro* after the laser irradiation (Fig. 2d and Fig. S29b, ESI†).

In order to verify the *in vitro* phototherapy efficacy of PDI-1S-4S NPs, 4T1 cells were co-cultured with PDI-1S-4S NPs having different concentrations for 12 h. After these co-cultured cells were irradiated with a NIR laser, they were incubated for another 6 h. According to the cell viability that was tested with the CCK-8 assay, the cell survival rate significantly was decreased with the increase of concentration of PDI-1S NPs or PDI-4S NPs under laser irradiation (Fig. 3a, b and Fig. S30, ESI†), which was also demonstrated through calcein AM/propidium iodide (PI) cell dead and alive staining (Fig. S31, ESI†). The superior PTT and PDT efficacies further proved that PDI-1S and PDI-4S NPs could be used as significant phototherapeutic agents.

In summary, a series of thionated PDIs were synthesized through a simple one-pot microwave reaction. The remarkable quenched fluorescence, rapid singlet oxygen generation, gradually reduced singlet oxygen quantum yields and enhanced photothermal conversion efficiencies of thionated PDIs were achieved through the increase of sulfur-substituted degree that adjusted their energy dissipation pathways. Furthermore, the excellent fluorescence and PA imaging, photodynamic and

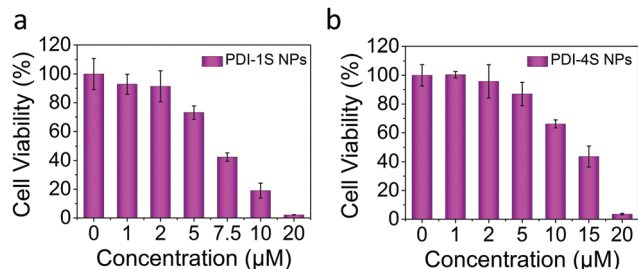


Fig. 3 Relative viabilities of cells after the laser irradiation (660 nm or 808 nm, 0.75 W cm<sup>-2</sup>, 5 min) with different concentrations of PDI-1S NPs and PDI-4S NPs.

photothermal therapy of representative thionated PDIs were verified *in vitro*. Therefore, this study might open a facile strategy to design theranostic agents with controllable photo-theranostics in on-demand biomedical applications.

This work was financially supported by the National Natural Science Foundation of China (52130309, 51903014 and 21774007), Beijing Natural Science Foundation (2202043), Fundamental Research Funds for the Central Universities (PT1811 and XK1802-2) and Joint Project of BRC-BC (XK2020-14).

## Conflicts of interest

There are no conflicts to declare.

## Notes and references

- 1 C. Chen, H. Ou, R. Liu and D. Ding, *Adv. Mater.*, 2019, **32**, 1806331.
- 2 H. Su, Y. Cui, F. Wang, W. Zhang, C. Zhang, R. Wang and H. Cui, *Biomater. Sci.*, 2021, **9**, 463–470.
- 3 S.-B. Wang, Z.-X. Chen, F. Gao, C. Zhang, M.-Z. Zou, J.-J. Ye, X. Zeng and X.-Z. Zhang, *Biomaterials*, 2020, **234**, 119772.
- 4 W. Cheng, H. Chen, C. Liu, C. Ji, G. Ma and M. Yin, *View*, 2020, **1**, 20200055.
- 5 C. Ji, W. Cheng, Q. Yuan, K. Müllen and M. Yin, *Acc. Chem. Res.*, 2019, **52**, 2266–2277.
- 6 Z. Liu, X. Wang, Q. Chen, F. Ma, Y. Huang, Y. Gao, Q. Deng, Z. Y. Qiao, X. Xing, J. Zhu, F. Lu and H. Wang, *Angew. Chem., Int. Ed.*, 2021, **60**, 16215–16223.
- 7 H. Li, Y. Zhang, B. Chen, Y. Wang, C. Teh, G. H. B. Ng, J. Meng, Z. Huang, W. Dong, M. Y. Tan, X. Sun, X. Li and J. Li, *ACS Appl. Bio Mater.*, 2019, **2**, 1569–1577.
- 8 Q. Fan, K. Cheng, Z. Yang, R. Zhang, M. Yang, X. Hu, X. Ma, L. Bu, X. Lu, X. Xiong, W. Huang, H. Zhao and Z. Cheng, *Adv. Mater.*, 2015, **27**, 843–847.
- 9 J. Li, C. Liu, Y. Hu, C. Ji, S. Li and M. Yin, *Theranostics*, 2020, **10**, 166–178.
- 10 M. Schulze, A. Steffen and F. Würthner, *Angew. Chem., Int. Ed.*, 2015, **54**, 1570–1573.
- 11 Q. Gong, J. Xing, Y. Huang, A. Wu, J. Yu and Q. Zhang, *ACS Appl. Bio Mater.*, 2020, **3**, 1607–1615.

- 12 P. Sun, X. Wang, G. Wang, W. Deng, Q. Shen, R. Jiang, W. Wang, Q. Fan and W. Huang, *J. Mater. Chem. B*, 2018, **6**, 3395–3403.
- 13 P. Sun, P. Yuan, G. Wang, W. Deng, S. Tian, C. Wang, X. Lu, W. Huang and Q. Fan, *Biomacromolecules*, 2017, **18**, 3375–3386.
- 14 V. N. Nguyen, Y. Yan, J. Zhao and J. Yoon, *Acc. Chem. Res.*, 2020, **54**, 207–220.
- 15 T. C. Pham, S. Heo, V.-N. Nguyen, M. W. Lee, J. Yoon and S. Lee, *ACS Appl. Mater. Interfaces*, 2021, **13**, 13949–13957.
- 16 L. A. Ortiz-Rodríguez and C. E. Crespo-Hernández, *Chem. Sci.*, 2020, **11**, 11113–11123.
- 17 L. A. Ortiz-Rodríguez, S. J. Hoehn, A. Loredó, L. Wang, H. Xiao and C. E. Crespo-Hernández, *J. Am. Chem. Soc.*, 2021, **143**, 2676–2681.
- 18 J. Tang, L. Wang, A. Loredó, C. Cole and H. Xiao, *Chem. Sci.*, 2020, **11**, 6701–6708.
- 19 A. J. Tilley, R. D. Pensack, T. S. Lee, B. Djukic, G. D. Scholes and D. S. Seferos, *J. Phys. Chem. C*, 2014, **118**, 9996–10004.
- 20 Z. Liu, Y. Gao, X. Jin, Q. Deng, Z. Yin, S. Tong, W. Qing and Y. Huang, *J. Mater. Chem. B*, 2020, **8**, 5535–5544.
- 21 V. N. Nguyen, S. J. Park, S. Qi, J. Ha, S. Heo, Y. Yim, G. Baek, C. S. Lim, D. J. Lee, H. M. Kim and J. Yoon, *Chem. Commun.*, 2020, **56**, 11489–11492.
- 22 V. N. Nguyen, S. Qi, S. Kim, N. Kwon, G. Kim, Y. Yim, S. Park and J. Yoon, *J. Am. Chem. Soc.*, 2019, **141**, 16243–16248.
- 23 P. Pahlavanlu, A. J. Tilley, B. T. McAllister and D. S. Seferos, *J. Org. Chem.*, 2017, **82**, 12337–12345.
- 24 S. Zhu, Z. Hu, R. Tian, B. C. Yung, Q. Yang, S. Zhao, D. O. Kiesewetter, G. Niu, H. Sun, A. L. Antaris and X. Chen, *Adv. Mater.*, 2018, **30**, 1802546.
- 25 B. Li, L. Lu, M. Zhao, Z. Lei and F. Zhang, *Angew. Chem., Int. Ed.*, 2018, **57**, 7483–7487.
- 26 D. Xi, M. Xiao, J. Cao, L. Zhao, N. Xu, S. Long, J. Fan, K. Shao, W. Sun, X. Yan and X. Peng, *Adv. Mater.*, 2020, **32**, 1907855.
- 27 K. Wen, L. Wu, X. Wu, Y. Lu, T. Duan, H. Ma, A. Peng, Q. Shi and H. Huang, *Angew. Chem., Int. Ed.*, 2020, **59**, 12756–12761.
- 28 M. Zhu, H. Zhang, G. Ran, D. N. Mangel, Y. Yao, R. Zhang, J. Tan, W. Zhang, J. Song, J. L. Sessler and J.-L. Zhang, *J. Am. Chem. Soc.*, 2021, **143**, 7541–7552.
- 29 C. Ji, L. Lai, P. Li, Z. Wu, W. Cheng and M. Yin, *Aggregate*, 2021, **2**, e39.
- 30 Z. Liu, H. Zou, Z. Zhao, P. Zhang, G.-G. Shan, R. T. K. Kwok, J. W. Y. Lam, L. Zheng and B. Z. Tang, *ACS Nano*, 2019, **13**, 11283–11293.
- 31 J. Zhang, W. Chen, R. Chen, X.-K. Liu, Y. Xiong, S. V. Kershaw, A. L. Rogach, C. Adachi, X. Zhang and C.-S. Lee, *Chem. Commun.*, 2016, **52**, 11744–11747.
- 32 F. Wu, L. Chen, L. Yue, K. Wang, K. Cheng, J. Chen, X. Luo and T. Zhang, *ACS Appl. Mater. Interfaces*, 2019, **11**, 21408–21416.
- 33 B. Wang, G. Feng, M. Seifrid, M. Wang, B. Liu and G. C. Bazan, *Angew. Chem., Int. Ed.*, 2017, **56**, 16063–16066.
- 34 R. K. Dubey, D. Inan, A. M. Philip, F. C. Grozema and W. F. Jager, *Chem. Commun.*, 2020, **56**, 5560–5563.
- 35 M. Miranda, C. A. Strassert, L. E. Dicelio and E. S. Román, *ACS Appl. Mater. Interfaces*, 2010, **2**, 1556–1560.
- 36 D. K. Roper, W. Ahn and M. Hoepfner, *J. Phys. Chem. C*, 2007, **111**, 3636–3641.
- 37 C. Liu, S. Zhang, J. Li, J. Wei, K. Müllen and M. Yin, *Angew. Chem., Int. Ed.*, 2019, **58**, 1638–1642.
- 38 Z. Lv, S. He, Y. Wang and X. Zhu, *Adv. Healthcare Mater.*, 2021, **10**, 2001806.